Structural, electronic properties and intramolecular hydrogen bonding of substituted 2-[(E)-imino methyl] benzenethiol in ground and first excited state by quantum chemical methods

ARTICLE *in* STRUCTURAL CHEMISTRY · SEPTEMBER 2013

Impact Factor: 1.84 · DOI: 10.1007/s11224-014-0391-9

3 AUTHORS, INCLUDING:

Fariba Mollania
University of Birjand
24 PUBLICATIONS **101** CITATIONS

Struct Chem (2014) 25:1187–1196
DOI 10.1007/s11224-014-0391-9

ORIGINAL RESEARCH

Structural, electronic properties and intramolecular hydrogen bonding of substituted 2-[(*E*)-imino methyl] benzenethiol in ground and first excited state by quantum chemical methods

Seyyed Jalal Seyyed Moosavi · Heidar Raissi · Fariba Mollania

Received: 14 September 2013 / Accepted: 4 January 2014 / Published online: 23 January 2014

Abstract Quantum chemical calculations of geometric structure, the intramolecular hydrogen bond, harmonic vibrational frequencies, NMR spin–spin coupling constants, and physical properties such as chemical potential and chemical hardness of the 2-(*E*)-imino methyl benzenethiol and its nineteen derivatives were carried out using density functional theory (DFT/B3LYP/6-311++G**) method in the gas phase and the water solution. Furthermore, the topological properties of the electron density distributions for S–H···N intramolecular hydrogen bond have been analyzed in terms of the Bader's theory of atoms in molecules (AIM). Natural bond orbital (NBO) analysis also performed for better understanding the nature of intramolecular interactions, the results of analysis by quantum theory of AIM and NBO method fairly supported the DFT results. Besides, MEP was performed by the DFT method. On the other hand, the aromaticity of the formed ring has been measured using several well-established indices of aromaticity such as nucleus-independent chemical shift, harmonic oscillator models of the aromaticity, para-delocalization index, average two-center indices, and aromatic fluctuation index. Also, the excited-state properties of intramolecular hydrogen bonding in these systems have been investigated theoretically using the time-dependent DFT method.

Keywords Electronic structure · DFT calculations · 2-[(*E*)-imino methyl] benzenethiol · Intramolecular hydrogen bond · Resonance parameters · Spin–spin coupling constants

Introduction

Compounds containing sulfur are omnipresent in nature. These compounds include thiophosphate pesticides, antibacterial agents (e.g., penicillins and cephalosporins), and important biological agents and metabolites (e.g., cysteine, homocysteine, glutathione, coenzyme A, and biotin). Sulfhydryl groups –SH are the most reactive in protein molecules (enzymatic and receptor), and the possibility of their chemical modification has an important regulative role [1–7]. Furthermore, sulfur-containing organic compounds and especially aromatic thiols have attracted enormous attention due to theirs potential applications in molecular electronic devices, taking advantage of their high conductivity and nonlinear optical properties [8–10]. Due to the importance and useful properties of Sulfur-containing compounds, the scope and application of these compounds have increased tremendously [11]. On the other hand, many chemical processes in these systems are modulated by the existence or the formation of intramolecular hydrogen bonds (HBs). The 2-(*E*)-imino methyl benzenethiol (IBT) (see Fig. 1) is one of the interesting benzenethiol derivatives, which involved in the S–H···N intramolecular hydrogen bonding. HB in its various aspects continues to be a topic of extreme scrutiny in various chemical and biological systems, as it plays a vital role in stabilizing molecular structures, and modulating specificity and speed of enzymatic reactions [12–15]. The hydrogen bonds can effect on the molecular structure and

Electronic supplementary material The online version of this article (doi:10.1007/s11224-014-0391-9) contains supplementary material, which is available to authorized users.

S. J. S. Moosavi (✉) · H. Raissi · F. Mollania
Chemistry Department, University of Birjand, Birjand, Iran
e-mail: sjsmoosavi@gmail.com

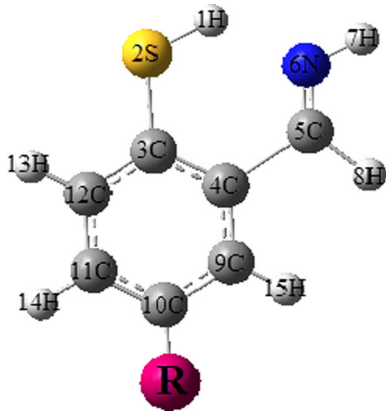

Fig. 1 Molecular structure with atom numbering scheme of IBT and IBTs derivative (R=F, Cl, Br, SH, CN, CHO, CH_2F, CH_2Cl, CH_2Br, CH_2OH, C_2H_5, $NHCH_3$, $NHCOCH_3$, CH_3, NO_2, CH_2COOH, CH_2OCH_3, and Ph)

properties in the excited state. On the other hand, time-dependent DFT (TD-DFT) method has been demonstrated as an effective way to theoretically study HBs in different electronic states [16–19].

In the present paper, our goal is to clarify the role of R substitution on the strength of the S–H···N hydrogen bridge, resonance and to estimate the energy of the S–H···N hydrogen bond in IBT and its derivatives. The effects of F, Cl, Br, SH, CN, CHO, CH_2F, CH_2Cl, CH_2Br, CH_2OH, C_2H_5, $NHCH_3$, $NHCOCH_3$, CH_3, NO_2, CH_2COOH, CH_2OCH_3, and Ph substitutions are examined. Furthermore, our study is directed to show how the properties derived from the topological analysis of the electron density can be applied for description of different aromaticity indices.

Computational details

All the calculations on IBT and its derivatives were performed by the use of Gaussian 03 program suite [20]. The geometry optimizations were carried out by B3LYP method using 6-311++G** basis set. Harmonic vibrational frequencies were estimated at the same levels to confirm the nature of the stationary points found and also to account for the zero-point vibrational energy (ZPVE) correction. The nature of the intramolecular hydrogen bond existing within IBT and its derivatives were studied by means of the Bader theory of atoms in molecules (AIM) [21, 22]. For an advanced understanding of the nature of intramolecular interactions, the natural bond orbital (NBO) analysis [23] was carried out using the NBO package included in Gaussian 03 suite of program. The contour plot for visualization of the NBO result was constructed on NBOView (Version1.1) [24] software package using the standard keywords implemented therein. The solvent effect was evaluated by employing the self-consistent reaction field (SCRF) method with the polarized continuum model (PCM) [25, 26]. The molecular orbital (MO) calculations such as harmonic oscillator model of aromaticity (HOMO)–LUMO were also performed on the IBT and its derivatives. In the present paper, the HB energies (E^*_{HB}) could be estimated from the properties of bond critical points. The simple relationship between HB energy and the potential energy density V(rcp) at the critical point corresponding to N···H contact was assigned to be $E^*_{HB} = 1/2V(\text{rcp})$ [27–30].

The aromaticity of the chelated rings of the different molecules was evaluated using the nucleus-independent chemical shift (NICS) method [30–32], the HOMA [33], the para delocalization index (PDI) [34], the average two-center index (ATI) [34, 35], and the aromatic fluctuation index (FLU) [36]. In the present work, the $R_{opt,\alpha}$ and δref parameters for evaluation of HOMA and FLU indices were calculated at B3LYP/6-311++G** level of theory (for CS, CC, and CN bonds: $R_{opt,CS} = 1.689$ Å, $R_{opt,CC} = 1.396$ Å, $R_{opt,CN} = 1.333$ Å, $\alpha_{CS} = 74.822$, $\alpha_{CC} = 88.253$, $\alpha_{CN} = 91.457$, $\delta_{ref,CS} = 4.626$, δrefCC = 1.385, and $\delta_{ref,CN} = 1.316$). Herein, some coupling constants (J_{H1-S2} and $J_{H1\cdots N6}$) have specifically been considered. Also for NMR calculations ^{1}H NMR chemical shifts δ_H were calculated using the GIAO method [37] in IBT and its derivatives. We used analytical procedure for calculations of spin–spin coupling constants that is available in the GAUSSIAN 03 program package [20].

Result and discussion

Optimized geometry parameters

The optimized molecular structure of IBT with the numbering scheme of the atoms obtained from Gaussview program [38] is shown in Fig. 1. The optimized structural parameters such as bond lengths, bond angles, Δ_{GEO} [39], and the energy of the intramolecular hydrogen bond of IBT and its derivatives are shown in Table 1. Comparing the geometrical parameters of IBT and its derivatives gives a clear understanding of substitution effects on structure and hydrogen-bond strength of these systems. The geometrical parameters showed that the N···S and N···H distances in chelated ring of IBT and its derivatives are in the range of 3.032–3.061 and 1.820–1.874 Å, respectively; significantly smaller than the sums of van der Waals radii of the involved atoms. The shortest S···N and N···H distances have been obtained for IBT system with NO_2 substitution (3.032 and 1.820 Å, respectively). According to energy values shown in Table 1, it can be seen that the greatest

Table 1 The geometric parameters (r and θ is in Å and °), Δ_{GEO}, and the energy of the intramolecular hydrogen bond (in kJ mol^{-1}), excitation energy (E), and oscillator strength (f) for IBT and its derivatives in gas phase (values in brackets refer to calculation at excited state)

R	S–H	N···H	S···N	SHN	Δ_{GEO}	E^*_{HB}	E	f
H	1.368 [1.398]	1.852 [1.546]	3.050 [2.839]	142.2 [149.2]	0.0097	−47.10	3.2737	0.0609
F	1.367 [1.503]	1.859 [1.223]	3.053 [2.670]	141.9 [156.5]	0.0088	−46.20	1.7425	0.0085
Cl	1.368 [1.514]	1.852 [1.208]	3.050 [2.666]	142.1 [156.7]	0.0096	−47.14	1.7636	0.0076
Br	1.368 [1.514]	1.851 [1.207]	3.049 [2.665]	142.1 [156.7]	0.0097	−47.22	1.7587	0.0071
SH	1.367 [1.389]	1.860 [1.843]	3.054 [3.054]	141.9 [141.4]	0.0088	−45.99	3.2972	0.0646
CN	1.371 [1.395]	1.831 [1.717]	3.038 [2.965]	142.7 [144.5]	0.0118	−50.27	3.5242	0.0614
CHO	1.372 [1.390]	1.830 [1.815]	3.037 [3.037]	142.7 [142.4]	0.0122	−50.44	3.6815	0.1071
CH_2F	1.369 [1.382]	1.844 [1.827]	3.046 [3.040]	142.4 [142.3]	0.0105	−48.29	3.6482	0.0707
CH_2Cl	1.369 [1.389]	1.845 [1.830]	3.046 [3.046]	142.3 [141.9]	0.0105	−48.07	3.6178	0.0714
CH_2OH	1.368 [1.385]	1.852 [1.840]	3.050 [3.051]	142.1 [141.7]	0.01	−47.03	3.6169	0.0724
CH_2CH_2OH	1.368 [1.409]	1.856 [1.549]	3.052 [2.853]	142.0 [149.5]	0.0091	−46.60	3.1962	0.0602
C_2H_5	1.368 [1.388]	1.855 [1.758]	3.051 [3.010]	142.0 [145.9]	0.0095	−46.68	3.4685	0.0729
$NHCH_3$	1.365 [1.414]	1.874 [1.637]	3.061 [2.930]	141.3 [147.5]	0.0075	−44.12	2.8108	0.0622
$NHCOCH_3$	1.368 [1.389]	1.855 [1.601]	3.051 [2.874]	142.0 [147.9]	0.0094	−46.67	3.3914	0.0757
CH_3	1.367 [1.386]	1.859 [1.830]	3.054 [3.043]	141.9 [141.9]	0.0092	−46.17	3.5499	0.073
CH_2Br	1.369 [1.385]	1.845 [1.807]	3.046 [3.026]	142.3 [142.6]	0.0105	−48.14	3.577	0.0731
NO_2	1.374 [1.385]	1.820 [1.796]	3.032 [3.020]	143.0 [143.1]	0.0132	−52.04	3.554	0.2763
CH_2COOH	1.369 [1.370]	1.851 [1.840]	3.050 [3.042]	142.2 [142.4]	0.0099	−47.23	3.6135	0.0717
CH_2OCH_3	[1.369]	1.850 [1.850]	3.050 [3.050]	142.2 [142.2]	0.01	−47.32	3.6651	0.075
Ph	1.368 [1.368]	1.855 [1.855]	3.052 [3.052]	142.0 [142.0]	0.0096	−46.74	3.4816	0.078

H-bond energy values belong to NO_2-substituted system; as a consequence, based on the obtained energy values, it is notable that this system has the strongest HB. Furthermore, taking IBT (R=H) as reference, the electron-withdrawing groups (e.g., Cl, Br, CN, CHO, CH_2F, CH_2Cl, CH_2Br, CH_2OH, CH_2OCH_3, and NO_2) decrease the S···N and N···H distances whereas the electron-donating substituents (e.g., CH_3, SH, C_2H_5, $NHCH_3$, CH_2CH_2OH, CH_2COOH, $NHCOCH_3$, and Ph) increase them. Opposite pattern is observed for S–H distances showing that the hydrogen bond in the case of electron-withdrawing substituents is relatively stronger than the parent molecule. The comparison between the electron-donating and the electron-withdrawing substitutions showed that the N···H distance for the electron-withdrawing substitutions is shorter than the corresponding values in the electron-donating substitutions. Moreover, the SHN bond angle can be an explanation for the HBs strength. In this case, the more nearness to 180°, the stronger is the HB. According to Table 1, it can be seen that the SHN bond angle in the NO_2 substitution is more than that of the other substituents, which proves that hydrogen bond in this molecule is vigorous.

It has been demonstrated that the geometrical parameters describing the elongation of the proton-donating bond may be normalized [39], according to the relation given below:

$$\Delta_{GEO} = \frac{(r_{X-H} - r^{\circ}_{X-H})}{r^{\circ}_{X-H}},$$

where r_{X-H} is the length of X–H bond within X–H···Y system and r°_{X-H} is the length of the free bond not involved in H-bonding (S–H). In other words, Δ_{GEO} is the elongation of X–H bond due to H-bridge formation in relation to the free X–H bond length. The geometrical parameter Δ_{GEO} correlates with H-bond energy; the correlation coefficient R amount to 0.996 and the linear regression is given by equation presented below:

$$\Delta_{GEO} = -0.0007E^*_{HB} - 0.0242,$$

Additionally, due to the existence of excellent linear correlation coefficients for dependency of Δ_{GEO} versus E^*_{HB}, intramolecular HB strength can be easily evaluated from geometrical properties.

AIM analysis

The atoms-in-molecules theory of Bader [21] (AIM) is also applied here to study the properties of the bond critical point of N···H contact and of the ring critical point (RCP) and to analyze dependencies between topological, energetic, and geometrical parameters. The calculated

Table 2 The selected topological parameters (in a.u.) and the charge transfer energies ($E^{(2)}_{LP(N)\rightarrow\sigma*SH}$, in kcal mol^{-1}) of investigated molecules in gas phase (values in brackets refer to calculation in water phase)

R	$\rho_{N\cdots H}$	$\nabla^2\rho_{N\cdots H}$	$E^{(2)}_{LP(N)\rightarrow\sigma*SH}$
H	0.04033 (0.04383)	0.10374 (0.10476)	18.25 (21.44)
F	0.03975 (0.04330)	0.10336 (0.10465)	17.76 (20.97)
Cl	0.04036 (0.04412)	0.10375 (0.10502)	18.30 (21.70)
Br	0.04041 (0.04405)	0.10376 (0.10492)	18.36 (21.66)
SH	0.03962 (0.04303)	0.10308 (0.104340	17.68 (20.77)
CN	0.04234 (0.04683)	0.10506 (0.10594)	20.03 (24.13)
CHO	0.04246 (0.04707)	0.10506 (0.10576)	20.09 (24.40)
CH_2F	0.04109 (0.04476)	0.10425 (0.10516)	18.93 (22.29)
CH_2Cl	0.04095 (0.04462)	0.10412 (0.10507)	18.81 (22.18)
CH_2OH	0.04029 (0.04406)	0.10361 (0.104800	18.19 (21.68)
CH_2CH_2OH	0.04001 (0.04321)	0.10338 (0.10433)	17.95 (20.94)
C_2H_5	0.04006 (0.04329)	0.10345 (0.10439)	17.85 (21.00)
$NHCH_3$	0.03841 (0.04140)	0.10201 (0.10324)	16.63 (19.33)
$NHCOCH_3$	0.04006 (0.04343)	0.10343 (0.10450)	18.60 (21.13)
CH_3	0.03974 (0.04295)	0.10310 (0.10414)	17.79 (20.72)
CH_2Br	0.04100 (0.04464)	0.10412 (0.10503)	18.87 (22.20)
NO_2	0.04346 (0.04895)	0.10553 (0.10607)	21.05 (25.83)
CH2COOH	0.04042 (0.04369)	0.10367 (0.10462)	18.39 (21.36)
CH_2OCH_3	0.04047 (0.04392)	0.10377 (0.10472)	18.41 (21.57)
Ph	0.04011 (0.04357)	0.10342 (0.10454)	18.03 (21.17)

topological parameters of IBT and its investigated derivatives are presented at Table 2. The maximum electron density observed for NO_2 substitution associated with the minimum N···H contact (1.820 Å). The shorter distance and greater electron density ($\rho_{N\cdots H}$) at N···H contact can be attributed to greater strength of hydrogen bond in NO_2 derivative of IBT. Also, the smallest value of $\rho_{N\cdots H}$ is predicted for $NHCH_3$ substitution, reflecting the weakest H···N interaction in $NHCH_3$-substituted system. In the electron-withdrawing substitutions, in comparison with the corresponding values of electron-donating substitutions, electron density is increased at BCP of N···H contact whereas electron density at BCP of S–H bond is decreased. From Table 2, we observe that for the electron-withdrawing substitutions, in comparison with the corresponding values of parent IBT, values of $\rho_{N\cdots H}$ and $\nabla^2\rho_{N\cdots H}$ have been increased. These values suggest that the HB strength in these derivatives is relatively stronger than the parent molecule. The calculated electron density properties for IBT and its derivatives show that N···H contacts have low ρ, $\nabla^2\rho_{BCP}$ and $-G_c/V_c < 1$ with $H_c < 0$, so they have partially covalent character in nature [39]. It means that S–H···N hydrogen bonds are medium in strength or even they are relatively strong. It is in line with the classification of hydrogen bonds given by Rozas et al. [40]. Furthermore, one can observe the monotonic AIM parameters' changes with the change of the N···H/S–H distance. V_C is always negative, and its modulus increases for shorter distances; G_C is always positive and increases if the distance decreases.

Numerous dependences are known from literature between the geometrical and topological parameters [12, 41, 42]. In this work, the distance–electron density linear relationship for N···H interaction is found. The corresponding correlation coefficient is very close to unity (0.999). Furthermore, the relationship between ρ_{BCP} and $\nabla^2\rho_{BCP}$ versus E^*_{HB} at N···H interaction is obtained. The correlation coefficients for these dependencies are very close to unit ($\sim$0.994). The characteristics of the other critical points are also analyzed. It was found that the RCP properties may be often treated as measures of the hydrogen-bond strength [14]. For the analyzed systems, the pseudo-ring containing S–H···N intramolecular hydrogen bond is created and hence the RCP exists. It is known that the greater electron density at RCP corresponds to the stronger intramolecular hydrogen bonding since there are correlations between the ∇^2_{RCP} values and the $\rho_{H\cdots N}$ values or the hydrogen bond energies [43]. For the investigated systems, there is also an excellent correlation between $\nabla^2\rho_{RCP}$ and $\rho_{N\cdots H}$ with a correlation coefficient of 0.999 (with derived equation as $\nabla^2\rho_{RCP} = 0.8815\ \rho_{N\cdots H} + 0.0353$). Also, there is a linear relationship between E^*_{HB} and $\nabla^2\rho_{RCP}$. The correlation coefficient for this dependency is very close to unit (0.998) (with equation as: $E^*_{HB} = -0.0006\nabla^2\rho_{RCP} + 0.0444$). The density of the

total energy of electrons (H) and its two components, the kinetic (G) and potential (V) electron energy densities, are estimated at proper RCPs. Our results show that there are linear relationships between E^*_{HB} and the total energy of electrons (H) and its two components (G and V). The dependence between the E^*_{HB} and G_C (V_C and H_C) is given as follows

$$y = -0.0004\,(0.0008,\ 0.0003)\,x + 0.0106\,(-0.0001,\ 0.0102)$$
$$R = 0.999(0.999,\ 0.998),$$

where y corresponds to E^*_{HB} and x corresponds to G_C (V_C and H_C) in kJ mol^{-1}. This implies that the properties of the RCP values could be very useful to estimate the strength of the intramolecular hydrogen bond. Their values permit us to have a better understanding of these novel correlations. The derived relationships from these graphs empower us to acquire other physically meaningful results.

In order to better elucidate hydrogen-bond strength, vibrational frequencies for all the derivatives were calculated. Our theoretical calculations show that the strengthening of hydrogen bond causes the frequencies of S–H stretching mode to shift to lower frequencies while in-plane and out-of-plane bending modes of S–H shifts to higher frequencies. The corresponding wavenumbers of the above modes are available upon request as Table S1 (supplementary material). Moreover, the linear correlation coefficient showing υ(S−H) dependency versus r_{S-H} ($\rho_{N\cdots H}$ and E^*_{HB}) is found to be 0.985 (0.991 and 0.991), with equation as:

$$y = -10792\,(-18712,\ 11.91)\,x + 17160\,(3149.8,\ 2956.3),$$

where y corresponds to υ(S−H) and x corresponds to $\rho_{N\cdots H}$ and E^*_{HB}. It means that υ(S−H) is a good description of the H-bond strength. Therefore, E^*_{HB} could be easily evaluated from ν(S–H). According to the stretching frequencies of the S–H bond for IBT and its derivatives, given in Table S1 (supplementary material), the red-shift of stretching modes are observed for conventional hydrogen bonds. The lengthening of the proton-donating bond as an effect of hydrogen bond formation is accompanied by this red-shift of the corresponding mode. Our theoretical results show the greatest shifts for electron-withdrawing substituents while the smallest shifts belong to electron-donating ones.

Natural bond orbital (NBO) analyses

The NBO analysis [23] provides an efficient method for studying intra- and inter-molecular bonding, and also offers a convenient basis for investigating charge transfer or conjugative interaction in molecular systems. Table 2 shows second-order perturbation stabilization energies, $E^{(2)}$, corresponding to charge transfer between nitrogen lone pair and σ^*_{SH} antibond ($E^{(2)}_{LP(N)\rightarrow\sigma^*SH}$, in kcal mol^{-1}). In the NBO analysis of hydrogen bonded systems, the charge transfer between the lone pairs of proton acceptor and antibonds of the proton donor is the most important. Hydrogen bonding causes an increase of the occupancy of the σ^*_{SH} antibond orbital and furthers the weakening and lengthening of the S–H bond. The value of $E^{(2)}_{LP(N)\rightarrow\sigma^*SH}$ depends on at least two factors: (a) the distance between N and H atoms (N···H) and (b) the donor ability of N atom. The maximum and minimum values of the σ^*_{SH} occupancy correspond to NO_2 and $NHCH_3$ substitutions, respectively. Consequently, the changes of occupation numbers of the nitrogen lone pair [LP(N)] orbital and σ^*_{SH} are in agreement with the charge transfer from LP(N) to σ^*_{SH} and hydrogen bond formation energy. The results of NBO analysis confirm that the H-bond strength in NO_2 substitution is stronger than the other derivatives because of more total charge transfer energy associated with the H-bond, and, therefore, more σ^*_{SH} occupancy in NO_2 substitution. The NBO analysis also describes the bonding in terms of the natural hybrid orbitals. The atomic charge distribution and percentage of the s-character of N_6 atom and the p-character of S_2 atom are investigated. The p-character of S_2 natural hybrid orbitals of σ^*_{SH} in NO_2 substitution ($sp^{4.64}$) is higher than the corresponding value of the parent molecule ($sp^{4.62}$), Our theoretical results show that the proton-donating bond length is essentially controlled by the p-character of these hybrid orbitals. Furthermore, in comparison with the parent molecule (37.61 %), the reduction of the s-character of the second lone pair of the N_6 orbital in the NO_2 substitution (37.40 %) accompanies with an increase in hydrogen bond formation energy. This is also the case for electron-withdrawing substitutions. Besides, in comparison with the IBT molecule, the least of p-character corresponding to S_2 natural hybrid orbitals of σ^*_{SH} ($sp^{4.93}$) is related to $NHCH_3$-substituted system. Also, most s-characters of the second lone pair of the N_6 orbital (37.69 %) belong to this molecule, which is another evidence for existence of the weakest H-bond in this molecule.

It is worth mentioning that NBO energy connected with $E^{(2)}_{LP(N)\rightarrow\sigma^*SH}$ overlap nicely correlates with other geometrical and topological parameters. For example, we found out that there is a good correlation between $E^{(2)}_{LP(N)\rightarrow\sigma^*SH}$ versus E^*_{HB}, $\rho_{N\cdots H}$ and r_{S-H}; correlation coefficients are 0.990, 0.990, and 0.985, respectively. This implies that the properties of the charge transfer between the lone pairs of proton acceptor and antibonds of proton donor could be very useful to estimate the strength of the intramolecular hydrogen bond. Figure 2 displays the NBO contour plots of

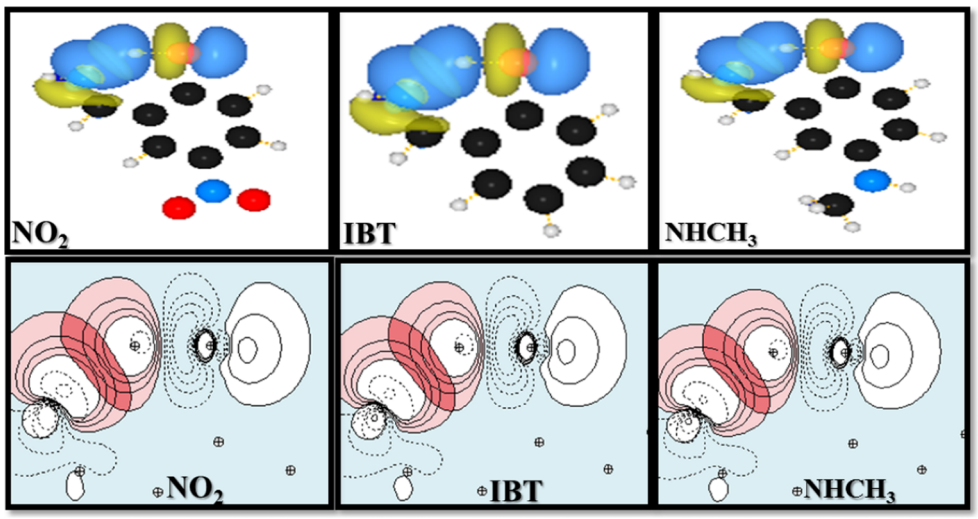

Fig. 2 NBO contour plots illustrating the interaction between the electron lone pair of nitrogen (N_6) with an antibonding S_2–H_1 orbital in parent molecule IBT and its $NHCH_3$ and NO_2 derivatives

the interaction between the electron lone pair of nitrogen (N_6) with an antibonding S_2–H_1 orbital in IBT and its NO_2 and $NHCH_3$ derivatives.

Resonance parameters

Results of the aromaticity calculations by aromatic indices are tabulated in Table S2 (Supplementary Material). There is a correlation between HOMA and FLU with a correlation coefficient of 0.842. The close correspondence found between HOMA and FLU can be attributed partly to the fact that FLU is constructed following, to some extent, the HOMA philosophy; that is, with the purpose of measuring the aromaticity by comparison with the values of a specific aromatic manifestation in indisputable aromatic systems such as benzene. Moreover, both indices concentrate on differences between contiguous atoms around the ring; though FLU measures cyclic electron fluctuation differences, HOMA compares bond lengths. From Table S2 (Supplementary Material), for CHO substitution, in comparison with the corresponding values of the other substitutions, HOMA value has been increased while the FLU value has been decreased. These values suggest that the local aromaticity in this substitution is more than the others. According to the results of HOMA calculations, it is clear that the system becomes more aromatic in the CHO, NO_2, CN, CH_2OH, CH_2F, CH_2Br, CH_2Cl, CH_2OCH_3, C_2H_5, Ph, and CH_3 substitutions with respect to the parent molecule. The correlations between different aromaticity indices and RCP properties have been checked for the investigated molecules. The correlation matrices for the correlations among aromaticity indices, E^*_{HB}, H_C, G_C, and V_C parameters have been reported in Table S3 (supplementary material). Among four aromaticity indices, HOMA, FLU, and PDI show the best linear relationship with E^*_{HB}, G_C, V_C and H_c properties, with correlation coefficients greater than 0.8 whereas the other indices are found to be less correlated with aromaticity indices. The exact observation shows that various aromaticity indices correlate with RCP properties in a different manner. The consequence of the π-electron delocalization within the investigated molecules are as follows: (I) the shortening of N···H and S···N distances; and (II) the shift of the proton toward the center of S···N contact. In the studied systems, π-electrons delocalization effect also plays an important role in the hydrogen bond strengthening. Thus, it can be stated that in comparison with the parent IBT and other derivatives, the highest π-electrons delocalization, the least of N···H and S···N distances and, subsequently, the strongest H-bond is related to NO_2–IBT.

Water solution

In order to investigate the geometry and the intramolecular hydrogen bond energy changes in the various IBT derivatives, optimization in water solution was carried out. The influence of the solvent on the strength of intramolecular hydrogen bonding is considered using the Tomasi's PCM [25, 26]. The calculated geometrical and topological parameters of IBT and its derivatives in water solution are collected in Tables 2, S1, and S4 (Supplementary Material). According to our theoretical results, the hydrogen-bond strength in solution is stronger than the gas phase. Also, it is seen that, in both phases, the electron-donating groups have weaker intramolecular HBs than the electron-withdrawing ones. Our findings reveal that the geometries of the studied systems do not change appreciably when solvent effects are taken into account. The structural parameters of IBT and its derivatives in gas phase and water solution predict an increase for S–H bond length but

the N···H distance was decreased with a shift from solution to the gas phase. The results of AIM and NBO calculations also confirm findings based on the geometrical data. Furthermore, the least value of E^*_{HB} is predicted for $NHCH_3$ substitution, reflecting the weakest N···H interaction in both water and gas phases. The highest H-bond strength is related to NO_2 substitution (see Table S4 Supplementary Material). In the present work, the R_{opt}, α, and δ_{ref} parameters for evaluation of HOMA and FLU indices [33, 34] are calculated at the B3LYP/6-311++G** level of theory in water solution (for CS, CC, and CN bonds: $R_{opt,CS} = 1.682$ Å, Ropt,CC = 1.397 Å, $R_{opt,CN} = 1.337$ Å, $\alpha_{CS} = 99.179$, $\alpha_{CC} = 89.650$ $\alpha_{CN} = 88.824$, $\delta_{ref,CS} = 4.626$, $\delta_{ref,CC} = 1.385$, $\delta_{ref,CN} = 1.316$). According to results of Table S2 (supplementary material), it can be mentioned that aromaticity for some R–IBTs with R=F, SH, $NHCH_3$, CH_3, $NHCOCH_3$, and CH_2CH_2OH is less than the parent molecule. The calculated dipole moments for IBT and its derivatives are presented at Table S5 (supplementary material). The results of this Table show that the $NHCH_3$ substitution creates the largest dipole moment while it is the smallest for IBT molecule with the SH electron-donating group. This may be explained by the consideration of charge values on the ring atoms. It can be mentioned that in the electron-donating substituents, S_2 and C_3 atoms carry the most negative charge but in NO_2 derivative they have the least charge density on S_2 and C_3 atoms. It is noticeable that the differences among the dipole moments in these derivatives can be attributed to the nature of substituents. In fact, high dipole moment illustrates the high reactivity of the title molecule. As a result of theoretical calculations, the dipole moment values of investigated molecules in the water solution are more than its corresponding values in the gas phase.

Nuclear magnetic resonance and spin–spin coupling constants investigations

The ^{1}H chemical shifts for IBT and its derivatives calculated by the gauge-included atomic orbital (GIAO) method are collected in Table S5 (supplementary material). The calculated chemical shielding is converted into chemical shifts (δ) by subtracting 31.76, the ^{1}H shielding of tetramethylsilane computed at the B3LYP/6-311++G** level of theory. The results of Table S5 (supplementary material) confirm that intramolecular hydrogen bonding will result in a decrease in diamagnetic shielding around the hydrogen nucleus. Therefore, the strengthening of hydrogen bond causes ^{1}H chemical shift of H to move down fields. For the investigated systems, there is also a good correlation between the ^{1}H chemical shifts parameters versus HB energy values (δ^1H_1 and E^*_{HB}) with the correlation coefficient of 0.986. As shown in Table S5(supplementary material), in gas phase, higher values of this parameter are obtained for some derivatives such as CH_2OCH_3-, NHC-OCH_3-, CH_2Cl-, CH_2Br-, CH_2F-, CN-, CHO-, and NO_2-substituted systems, which prove that in these substitutions the hydrogen bond formation has greater influence on H atom movement toward the proton acceptor atom and also more electronic charge distribution. This is also the case for NO_2, CH_2COOH, CHO, CN, CH_2F, CH_2Br, CH_2Cl, CH_2OH, and CH_2OCH_3 substitutions in water solution.

Another aim of the present work is to describe a new tool which allows representing the electron density shift in those regions where H-bonding formation is expected. Indeed, a better understanding of NMR J-coupling constants would much benefit for closer study of H-bonding formation. Herein, the substituent effect on spin–spin coupling constant across N···H hydrogen bond has been investigated. With regard to Table S5 (supplementary material), it is important to emphasize that in both phases, the least $J_{H1\cdots N6}$ values belong to $NHCH_3$–IBT, which has the weakest HB. It should be noted that, as hydrogen bonding becomes stronger, the value of spin–spin coupling constant (J) increases (see Tables 1 and S5). Moreover, our theoretical results show that electron-withdrawing substitutions enhance the values of the $J_{H1\cdots N6}$ whereas this behavior for electron-donating substitutions is vice versa. From the Table S5 (Supplementary Material), the maximum value of $J_{H1\cdots N6}$ coupling constant in gas phase and solution corresponds to NO_2–IBT and CHO–IBT, respectively, which can be attributed to increasing π-electron cloud of ring by these electron-withdrawing substituents. Besides, it can be concluded that stronger hydrogen bond leads to more spin–spin coupling constant value between the participating atoms in S–H···N interaction. The results of our theoretical calculations confirm that there is a linear relationship between $J_{H1\cdots N6}$ coupling constant and E^*_{HB} (with equation as: $J_{H1\cdots N6} = 0.0376E^*_{HB} - 6.2794$ with $R = 0.951$, gas phase; $J_{H1\cdots N6} = 0.0173E^*_{HB} - 7.2674$ with $R = 0.824$, solution). Also, there is a linear correlation between J_{H1-S2} and E^*_{HB} (the linear correlation coefficient of 0.971 and 0.952, respectively, in gas phase and water solution) with derived equations as:

$$J_{H1-S2} = 0.0744(0.0849)\,E^*_{HB} + 36.538(37.592),$$

This fact also is in line with the earlier studies pointing out that J_{H1-S2} may be treated as a good measure of the hydrogen-bond strength for intramolecular hydrogen bonds [12].

Frontier MO energies and chemical indices

Energies of the lowest unoccupied MO ($E_{LUMO}E_{LUMO}$) and the highest occupied MO (E_{HOMO}), frontier Mo energy gap,

$\Delta E_{HOMO-LUMO}$, chemical hardness, and chemical potential of IBT and its derivatives are listed in Table S5 (supplementary material). The eigenvalues of HOMO and LUMO and their energy gap reflect the activity of the molecule. [44]. A comparison of the energies of the HOMO and LUMO orbitals (Table S5 Supplementary Material) reveals that the energy difference between the energy levels of HOMO and LUMO is the lowest in IBT system with $NHCH_3$ substitution and the highest in the parent molecule and IBT–CH_2F, in comparison with the other derivatives. Using HOMO and LUMO energy values for a molecule, the chemical potential (μ) and global hardness (η) can be calculated as follows [45–47]:

$$\eta = \frac{E_{LUMO} - E_{HOMO}}{2}, \quad \mu = \frac{E_{LUMO} + E_{HOMO}}{2},$$

The chemical hardness is a good indicator of the chemical stability. The molecules having a small energy gap are known as soft and those having a large energy gap are known as hard molecules. Due to the Pearson's maximum hardness principle (MHP) [48] which points out that the minimum energy structure has the maximum chemical hardness, with only a few exceptions, it seems that some of electron-withdrawing groups (e.g., Br, CN, CHO, CH_2Cl, CH_2Br, CH_2OH, CH_2OCH3, and NO_2) and the number of electron-donating substituents (e.g., F, C_2H_5, $NHCH_3$, CH_2CH_2OH, and CH_2COOH) obey from this principle.

Molecular electrostatic potential

The Molecular electrostatic potential (MEP) is a useful property to study of reactivity that an approaching electrophile will be attracted to negative regions (where the electron distribution effect is dominant). In the majority of the MEP, while the maximum negative region preferred its site for electrophilic attack indications as red color, the maximum positive region preferred its site for nucleophilic attack symptoms as blue color. Such mapped electrostatic potential surfaces have been plotted for IBT and its $NHCH_3$ and NO_2 derivatives (see Fig. 3). In MEP map of IBT and its $NHCH_3$ derivative, the surfaces over the N atoms and phenyl ring representing the maximum negative electrostatic potential, and the surfaces over the S atom and hydrogen atoms of out of ring indicating maximum positive electrostatic potential, therefore, may be the sites of electrophilic and nucleophilic reactions, respectively (see Fig. 3). For NO_2 substitution, the MEP plot shows a strong positive electrostatic potential (electron poor—blue color) and weak negative electrostatic potential (electron rich—red color), which occur at the hydrogen atoms of out of ring and the oxygen atoms of NO_2 group, respectively.

Hydrogen bond in the excited state

The salient geometric, the electronic excitation energies as well as the corresponding oscillator strengths of the first excited states (S_1) for IBT and its derivatives calculated using the TD-DFT method are presented in Table 1. It can be clearly seen that the H-bond strength is increased considerably in the $\pi\pi^*$ state, compared to ground state (S_0). Our theoretical results showed that the distance between the S and N atoms in the S_0 is longer than the corresponding value in S_1. From Table 1 it can be observed that for unsubstituted IBT, the distance between H and S atoms in intramolecular hydrogen bonding S–H···N is significantly lengthened from 1.368 Å in the ground state to 1.398 Å in the excited state. In order to better highlight this point, an effort has been made to explore the N···H and S···N distances for parent molecule. These distances are drastically reduced from 1.852 Å in the ground state to 1.546 Å in the excited state for N···H interaction and from 3.050 Å in the ground state to 2.839 Å in the excited state for S···N distance (see Table 1). Since SHO bond angle can be an explanation for the HBs strength, it is noteworthy that for IBT, the value of this angle has increased from 142.2° in the ground state to 149.2° in the excited state, which is another reason for existence of stronger HB in this

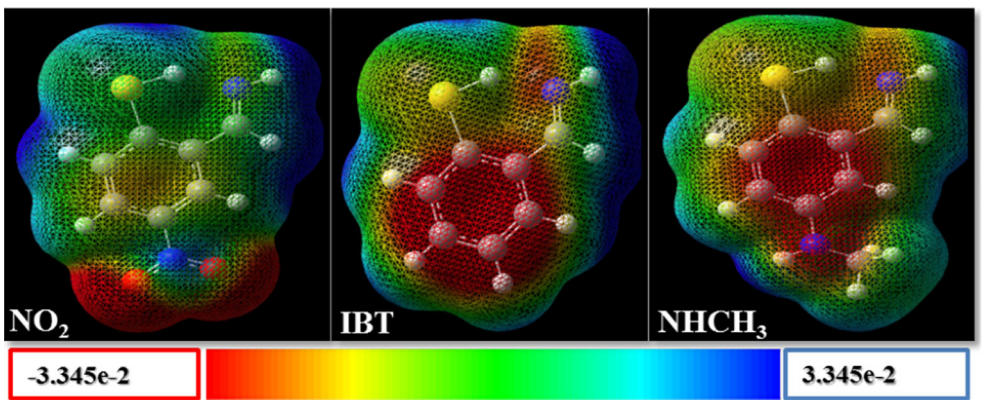

Fig. 3 Electron density isosurface mapped with electrostatic potential surface for IBT and its $NHCH_3$ and NO_2 derivatives

molecule in the excited state. Meanwhile, for all the IBT derivatives, the values of covalent SH bond length and SHO bond angle increase whereas the values of N···H and S···N distances decrease, which confirm that the intramolecular hydrogen bond S–H···N=C is significantly strengthened upon excitation to the S_1 state. Inspection of Table 1 reveals clearly that the electronic excitation energy of the S_1 state of IBT and its derivatives is in ranges of 1.7425–3.6815 eV. As it is obvious from Table 1, the oscillator strength of the investigated systems in S_1 state is in the range of 0.0071–0.2763.

Conclusion

The geometries, electronic structures, vibrational frequencies, intramolecular hydrogen-bond strength, and physical properties such as dipole moment, chemical potential, and chemical hardness of substituted IBT compound were investigated using DFT calculations. Furthermore, the electronic excited-state properties of IBT and its derivatives were investigated by TD-DFT method. The results obtained from DFT calculations and the topological parameters derived from the Bader theory suggested that the stronger HB can lead to lengthening the S–H bond and shortening the S···N and N···H distances. It has been shown that substituents attached to the IBT moiety influence both the intramolecular HB as well as quasi-aromatic character of the quasi-ring formed due to HB formation. Our results showed that in comparison with IBT molecule, the N···H and S···N distances are decreased for electron-withdrawing groups and are increased for electron-donating substituents. It was also found that the characteristics of RCP are good descriptors of the H-bond strength. The influence of substituents on H-bond strength was analyzed. The electron-withdrawing and electron-donating substituents may influence the π-electron delocalization. Moreover, the calculated electron densities and Laplacian properties of IBT and its derivatives illustrate that N···H bonding in all the studied molecules has lower ρ and positive $\nabla^2\rho$ values; but the corresponding H_{BCP} values are negative, which means the interaction is at least partly covalent. Our theoretical calculations showed that the hydrogen bond strength in the gas phase is weaker than the water solution.

References

1. Allison LA, Keddington J, Shoup RE (1983) Liquid chromatographic behavior of biological thiols and the corresponding disulfides. J Liquid Chromatogr 6:1785–1798
2. Yamashita G, Rabenstein D (1989) Determination of penicillamine, penicillamine disulfide and penicillamine-glutathione mixed disulfide by high-performance liquid chromatography with electrochemical detection. J Chromatogr 491:341–354
3. Sun Y, Smith DL, Shoup RE (1991) Simultaneous detection of thiol- and disulfide-containing peptides by electrochemical high-performance liquid chromatography with identification by mass spectrometry. Anal Biochem 197:69–76
4. Perrett D, Drury PL (1982) The determination of captopril in physiological fluids using high performance liquid chromatography with electrochemical detection. J Liquid Chromatogr 5:97–110
5. Baker DH (1986) Utilization of isomers and analogs of amino acids and other sulfur-containing compounds. Prog Food Nutr Sci 10:133–178
6. Cappiello M, Vilardo PG, Micheli V, Jacomelli G, Banditelli S, Leverenz V, Giblin FJ, del Corso A, Mura U (2000) Thiol disulfide exchange modulates the activity of aldose reductase in intact bovine lens as a response to oxidative stress. Exp Eye Res 70:795–803
7. Bumm LA, Arnold JJ, Cygan MT, Dunbar TD, Burgin TP, Jones L II, Allara DL, Tour JM, Weiss PS (1996) Are single molecular wires conducting? Science 271:1705–1707
8. Schreiber F (2000) Structure and growth of self-assembling monolayers. Prog Surf Sci 65:151–257
9. Reed MA, Zhou C, Muller CJ, Burgin TP, Tour JM (1997) Conductance of a molecular junction. Science 278:252–254
10. Carron KT, Hurley LG (1991) Axial and azimuthal angle determination with surface-enhanced Raman spectroscopy: thiophenol on copper, silver, and gold metal surfaces. J Phys Chem 95:9979–9984
11. Banwart WL, Bremner JM (1975) Formation of volatile sulfur compounds by microbial decomposition of sulfur-containing amino acids in soils. Soil Biol Biochem 7:359–364
12. Raissi H, Khoshbin Z, Mollania F (2013) The analysis of structural and electronic properties for assessment of intramolecular hydrogen bond (IMHB) interaction: a comprehensive study into the effect of substitution on intramolecular hydrogen bond of 4-nitropyridine-3-thiol in ground and electronic excited state. Struct Chem. doi:10.1007/s11224-013-0314-1
13. Jeffrey GA (1997) An introduction to hydrogen bonding. Oxford University Press, New York
14. Raissi H, Yoosefian M, Mollania F (2012) Comprehensive study of the interaction between hydrogen halides and methanol derivatives. Int J Quantum Chem 112:2782–2786
15. Kuhn B, Mohr P, Stahl M (2010) Intramolecular hydrogen bonding in medicinal chemistry. J Med Chem 53:2601–2611
16. Zhao G, Yu F, Zhang M, Northrop B, Yang H, Han K, Stang P (2011) Substituent effects on the intramolecular charge transfer and fluorescence of bimetallic platinum complexes. J Phys Chem A 115:6390–6393
17. Cao X, Liu C, Liu Y (2012) Theoretical studies on the mechanism of cyclic nucleotide monophosphate hydrolysis within phosphodiesterase. Theor Comput Chem 11:573–586
18. Raymo FM, Bartberger MD, Houk KN, Stoddart JF (2001) The magnitude of [C–H···O] hydrogen bonding in molecular and supramolecular assemblies. J Am Chem Soc 123:9264–9267
19. Zhao GJ, Han KL (2012) Hydrogen bonding in the electronic excited state. Acc Chem Res 45:404–413
20. Frisch MJ, Trucks GW, Schlegel HB, Scuseria GE, Robb MA, Cheeseman JR, Montgomery JA, Vreven Jr T, Kudin KN, Burant JC, Millam JM, Iyengar SS, Tomasi J, Barone V, Mennucci B, Cossi M, Scalmani G, Rega N, Petersson GA, Nakatsuji H, Hada M, Ehara M, Toyota K, Fukuda R, Hasegawa J, Ishida M, Nakajima T, Honda Y, Kitao O, Nakai H, Klene M, Li X, Knox JE, Hratchian HP, Cross JB, Adamo C, Jaramillo J, Gomperts R, Stratmann RE, Yazyev O, Austin AJ, Cammi R, Pomelli C, Ochterski JW, Ayala PY, Morokuma K, Voth GA, Salvador P,

Dannenberg JJ, Zakrzewski VG, Dapprich S, Daniels AD, Strain MC, Farkas O, Malick DK, Rabuck AD, Raghavachari K, Foresman JB, Ortiz JV, Cui Q, Baboul AG, Clifford S, Cioslowski J, Stefanov BB, Liu G, Liashenko A, Piskorz P, Komaromi I, Martin RL, Fox DJ, Keith T, Al-Laham M A, Peng CY, Nanayakkara A, Challacombe M, Gill PMW, Johnson B, Chen W, Wong MW, Gonzalez C, Pople JA (2003) Gaussian 03, Revision C.02 (or D.01). Gaussian Inc., Pittsburgh
21. Bader RFW (1990) Atoms in molecules—a quantum theory. Clarendon Press, Oxford
22. AIM (2000) AIM2000 designed by Friedrich Biegler-König. University of Applied Sciences, Bielefeld
23. Glendening ED, Reed AE, Carpenter JE, Weinhold F (1992) NBO, Version 3.1. Gaussian Inc, Pittsburgh
24. Wendt M, Weinhold F (2001) NBOView 1.0. Theoretical Chemistry Institute, University of Wisconsin, Madison
25. Cossi M, Barone V, Cammi J (1996) Ab initio study of solvated molecules: a new implementation of the polarizable continuum model. Chem Phys Lett 255:327–335
26. Miertus S, Scrocco E, Tomasi J (1981) Electrostatic interaction of a solute with a continuum. A direct utilizaion of AB initio molecular potentials for the prevision of solvent effects. Chem Phys 55:117–129
27. Espinosa E, Molins E (2000) Retrieving interaction potentials from the topology of the electron density distribution: the case of hydrogen bonds. J Chem Phys 113:5686–5694
28. Espionsa E, Souhassou M, Lachekar H, Lecomte C (1999) Topological analysis of the electron density in hydrogen bonds. Acta Crystallogr B 55:563–572
29. Abramov YA (1997) On the possibility of kinetic energy density evaluation from the experimental electron-density distribution. Acta Crystallogr A 53:264–272
30. Chen Z, Wannere CS, Corminboeuf C, Puchta R, PvR Schleyer (2005) Nucleus-independent chemical shifts (NICS) as an aromaticity criterion. Chem Rev 105:3842–3888
31. Kruszewski J, Krygowski TM (1972) Definition of aromaticity basing on the harmonic oscillator model. Tetrahedron Lett 13:3839–3842
32. PvR Schleyer, Maerker C, Dransfeld A, Jiao H, van Eikema Hommes NJR (1996) Nucleus-independent chemical shifts: a simple and efficient aromaticity probe. J Am Chem Soc 118:6317–6318
33. Krygowski TM, Cyranski MK (1996) Separation of the energetic and geometric contributions to the aromaticity of π-electron carbocyclics. Tetrahedron 52:1713–1722
34. Poater J, Fradera X, Duran M, Solà M (2003) Three-dimensional structure-activity relationship modeling of cross-reactivities of a polyclonal antibody against pyrene by comparative molecular field analysis. Chem Eur J 9:400–406
35. Bultinck P, Ponec R, Van Damme S (2005) Multicenter bond indices as a new measure of aromaticity in polycyclic aromatic hydrocarbons. J Phys Org Chem 18:706–718
36. Matito E, Duran M, Solà M (2005) The aromatic fluctuation index (FLU): a new aromaticity index based on electron delocalization. J Chem Phys 122:014109
37. Wolinski K, Hinton JF, Pulay P (1990) Efficient implementation of the gaugein- dependent atomic orbital method for NMR chemical shift calculations. J Am Chem Soc 112:8251–8260
38. Frisch A, Nielson AB, Holder AJ (2000) Gaussview user manual. Gaussian Inc., Pittsburgh
39. Grabowski SJ (2001) Hydrogen bonding strength—measures based on geometric and topological parameters. J Phys Chem A 105:10739–10746
40. Rozas I, Alkorta I, Elguero J (1997) Unusual hydrogen bonds: H$\cdots\pi$ interactions. J Phys Chem A 101:9457–9463
41. Raissi H, Yoosefian M, Mollania F (2012) Hydrogen bond studies in substituted imino-acetaldehyde oxime. Computational and theoretical chemistry 996:68–75
42. Raissi H, Khanmohamadi A, Mollania F (2013) A theoretical DFT study on the structural parameters and intramolecular hydrogen-bond strength in substituted (*Z*)-*N*-(thionitrosomethylene) thiohydroxylamine systems. Bull Chem Soc Jpn. doi:10.1246/bcsj.20120242
43. Raissi H, Farzad F, Eslamdoost S, Mollania F (2013) Conformational properties and intramolecular hydrogen bonding of 3-amino-propeneselenal: an ab initio and density functional theory studies. J Theor Comput Chem 12:1350025–1350042
44. Gunasekaran S, Balaji RA, Kumeresan S, Anand G, Srinivasan S (2008) Can J Anal Sci Spectrosc 53:149–162
45. Koopmans TA (1934) Über die Zuordnung von Wellenfunktionen und Eigenwerten zu den Einzelnen Elektronen Eines atoms. Physica 1:104–113
46. Pearson RG (1985) Absolute electronegativity and absolute hardness of Lewis acids and bases. J Am Chem Soc 107:6801–6806
47. Parr RG, Chattaraj PK (1991) Principle of maximum hardness. J Am Chem Soc 113:1854–1855
48. Pearson RG (2001) Hard and Soft Acids and Bases. Dowden (Hutchison & Ross), Stroudsburg